Phenomenological Theory of Low-Voltage Electroporation. Electric Field Calculations

István P. Sugár,*,† James Lindesay,‡ and Robert E. Schmukler§

Departments of Biomathematical Sciences and Physiology/Biophysics, Mount Sinai School of Medicine, New York, New York 10029, Computational Physics Laboratory, Howard University, Washington, DC 20059, Stanford Linear Accelerator Center, Stanford University, Stanford, California 94309, Pore² Bioengineering, 19212 Orbit Drive, Gaithersburg, Maryland 20879, and Drexel University, Philadelphia, Pennsylvania 19104

Received: October 31, 2002; In Final Form: February 6, 2003

In common electroporators, cells can be transfected with foreign genes by applying a 150−700 V pulse on the cell suspension. Because of Joule heating, the cell survival rate is 10−20% in these elecroporators. In a recently developed electroporator, termed the low-voltage electroporator (LVEP), cells are partially embedded in the pores of a micropore filter. In LVEP, cells can be transfected by applying 25 V or less under normal physiological conditions at room temperature. The large increase in current density in the filter pores, produced by the reduction of current shunt pathways around each embedded cell, amplifies 1000-fold the local electric field across the filter and results in a high-enough transmembrane voltage for cell electroporation. The Joule heat generated in the filter pore is quickly dissipated toward the bulk solution on each side of the filter, and thus cell survival in the low-voltage electroporator is very high, about 98%, while the transfection efficiency for embedded cells is above 90%. In this paper, the phenomenological theory of LVEP is developed. The transmembrane voltage is calculated along the membrane of the cell for three different cell geometries. The cell is either fully, partially, or not embedded in the filter pore. By means of the calculated transmembrane voltage, the distribution of electropores along the cell membrane is estimated. In agreement with the experimental results, cells partially embedded in the filter pore can be electroporated by as low as 1.8−3.5 V of applied voltage. In the case of 25 V applied voltage, 90% of the cell surface can be electroporated if the cell penetrates further than half of the length of the filter pore.

1. Introduction

Biological membranes are known to become transiently more permeable by the action of short electric field pulses[1−4] when the threshold value of the transmembrane voltage, about 0.5−1 V, is exceeded. (The transmembrane voltage is defined by the potential difference between the inner and outer surfaces of the cell membrane.) This phenomenon is called electroporation or electropermeabilization, and it can be used to transfect cells with foreign genes.[5] Electroporation of biological cells is commonly carried out in a cell suspension using a parallel plate capacitor chamber.[6] The field between the plates is essentially homogeneous because the cell density is low. The voltage required for electroporation varies from 150 to 700 V across a 0.2 cm gap of physiologic solution (∼0.15 M NaCl). The applied voltage depends on factors such as the spacing between the capacitor plates, the cell type, and solution temperature. The field strengths needed for suspension electroporation normally vary between 750 and 2000 V/cm. The resulting current produced by these fields in the low-resistivity physiologic solution is in the range of 25−100 A. Substantial Joule heating, electrode products, and solution electrolysis are byproducts produced by these fields in cell suspension,[7] and thus the cell survival rate is low. For COS-7 cells, the survival rate in suspension experiments varies from 10% (ref 8) to 20% (ref 9). These survival rates are in agreement with the rates quoted by commercial companies for their systems (personal communications with BTX Corp., Life Technologies, Inc., and Savant/E-C Apparatus, Inc.)

Recently, an alternative to cell suspension electroporation (SEP), the method of low-voltage electroporation (LVEP), was introduced.[10−16] A schematic of the low-voltage electroporator (LVEP) is shown in Figure 1.[17] The vertical chamber consists of two mirror-image halves. The inside diameter of the cylindrical chamber is 1 cm, and cylindrical porous carbon electrodes enclose the upper and lower ends of the chamber. The carbon electrodes apply the input signal and are separated by 2 cm. This produces a cylindrical measurement volume with dimension of 1 cm in diameter and 2 cm in length. A polycarbonate Nuclepore filter (its plane aligned perpendicular to the symmetry axis of the chamber) is sealed into the center of the chamber, and the cells are then embedded in the filter pores (see enlargement in Figure 1) by using a hydrostatic pressure of 25−30 mmHg. In LVEP, as low as 2−25 V of applied voltage is sufficient to induce electroporation because 40% of the applied voltage drops in the 13 μm long micropores of the filter.[17] The average field across the entire chamber for 10 V input is less than 5 V/cm, while the average field across the filter with cells is about 3000 V/cm. Thus, the field in a LVEP is highly inhomogeneous, amplified about 1000 times in conjuntion with the increase in current density through the filter pores. However, the current produced in this system is only 25−50 mA. The bulk temperature increase caused by a 90 ms pulse of 10 V is less than 0.003 °C, and the local Joule heating generated in the filter pore is dissipated in less than 0.3 ms (ref 16). Because of the negligibly small Joule heating, the cell survival rate is about 98% (refs 12 and 16).

The development of the phenomenological theory of SEP started 30 years ago. The transmembrane voltage around a

† Mount Sinai School of Medicine.
‡ Howard University and Stanford University.
§ Pore² Bioengineering and Drexel University.

10.1021/jp022343k CCC: $25.00
Published on Web 03/26/2003

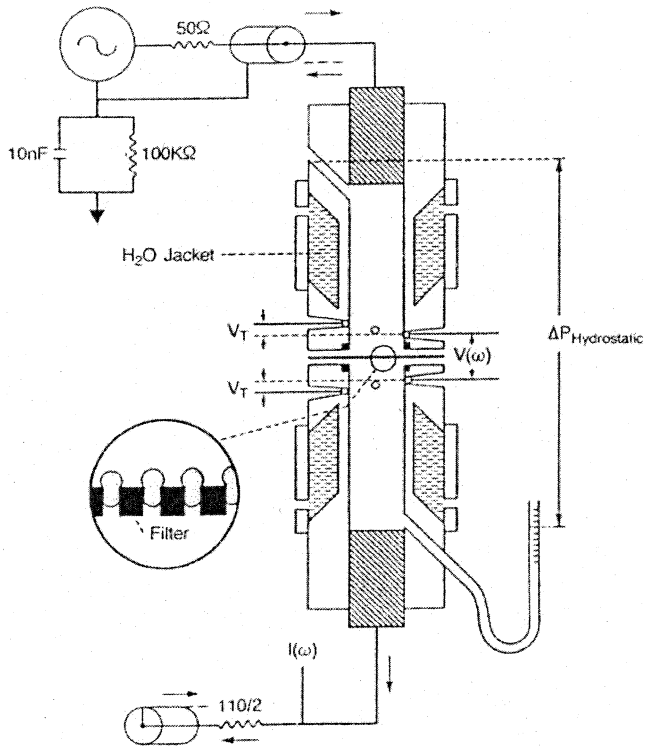

Figure 1. Schematic of the low-voltage electroporator (LVEP). Shaded areas mark the cylindrical carbon electrodes at the top and the bottom of the vertical chamber. The chamber is divided by a micropore filter. The plane of the filter aligned perpendicular to the symmetry axis of the cylindrical chamber is marked by a heavy solid line. The inset shows a magnified part of the filter with cells partially embedded in the micropores. Note that in the figure the chamber is stretched along its symmetry axis. In reality the chamber's inner length and diameter is 2 and 1 cm, respectively.

spherical cell placed into a constant, subcritical electric field, $V(\theta)$, was determined by solving the Laplace equation.[18,19] The field is subcritical as long as the absolute value of the transmembrane voltage is below the critical value, $V_{cr} \approx 0.5-1$ V. When the field is switched on at time $t = 0$, the steady-state transmembrane voltage, $V(\theta)$, is attained after the charging of the membrane. In this case, the solution can be separated to the steady-state and transient part, $f(t)$, as follows:

$$V(\theta,t) = [V(\theta)][f(t)] = [1.5RE_o\cos(\theta)][1 - e^{-t/\tau}] \quad (1)$$

where R is the radius of the cell, E_o is the field strength far from the cell, θ is the angle (azimuthal angle) between the direction of E_o and the vector directed from the center of the cell to the considered membrane segment, and τ is the membrane's charging time constant. According to eq 1, the absolute value of $V(\theta)$ is maximal at the poles of the cell, while it is zero at the equator.

In the case of supracritical fields, when electroporation takes place, however, there is no closed form solution of the Laplace equation. The azimuthal dependence of the transmembrane voltage, $V_{exp}(\theta,t)$, was measured on a spherical sea urchin egg stained with voltage-sensitive fluorescent dye at different time points after the application of a supracritical electric field.[20−22] These measurements showed that (i) those regions of the cell membrane that would experience supracritical transmembrane voltage appear to be porated within less than 1 μs and (ii) the transmembrane voltage remains symmetrical around the z-axis (the axis going through the poles of the egg), although it decreases significantly within a certain range around the pole.

We notice that the transmembrane voltage, $V(\theta,t)$, can be calculated by means of eq 1 not only at subcritical pulses but also at supracritical pulses if the cell membrane is assumed to be unporated. In reality, pore formation takes place where the absolute value of this calculated transmembrane voltage exceeds the critical voltage, V_{cr}. In the case of supracritical electric pulses, the phenomenological theory of SEP has been developed by Kinoshita and co-workers. They assumed that the probability of pore formation is directly proportional to $|V(\theta,t)| - V_{cr}$, where $V(\theta,t)$ is defined by eq 1. Thus, at any time t after the application of the supracritical pulse, the excess specific conductivity in the porated region of the membrane, $\Delta\sigma_m(\theta,t)$, is

$$\Delta\sigma_m(\theta,t) = \Delta\sigma_m(\theta_o,t)\frac{|V(\theta,t)| - V_{cr}}{|V(\theta_o,t)| - V_{cr}} = \Delta\sigma_m(\theta_o,t)\frac{|V(\theta)|f(t) - V_{cr}}{|V(\theta_o)|f(t) - V_{cr}} \quad (2)$$

where at $\theta = \theta_o$ $|V(\theta)|$ assumes its global maximum. By using the above function for the excess membrane specific conductivity, Hibino et al.[21,22] solved the Laplace equation numerically. The solution was in accordance with the measured transmembrane voltage, $V_{exp}(\theta,t)$. At any given time, t, the excess specific conductivity of the membrane at the pole, $\Delta\sigma_m(0,t)$, was the only adjusted parameter of the theory of SEP. The analysis of the experimental data revealed that $\Delta\sigma_m(0,t)$ gradually increased as long as the electric field was on. After switching off the field, the decrease of $\Delta\sigma_m(0,t)$ could be described by two exponentials with time constants of 7 and 500 μs. We note that the above theory is more complicated in the case of an asymmetric electroporation model.[22]

In this paper, after defining the geometrical and material parameters of the system in the Model section, we present the solutions of the Laplace equation in the Results section for different lengths of cell penetration into the filter pore. In the Discussion section, the calculated electric field is compared with the field around a single spherical cell in cell suspension, and the importance of the current density amplification (CDA) is discussed. The distribution of the electropores along the membrane is calculated for different cell geometries. The calculated minimal applied voltage needed to induce electroporation is compared with the available experimental result, and the efficiency of electroporation is defined and calculated for different cell geometries.

2. Model

2.1. Geometry of the Model of Low-Voltage Electroporator. The LVEP can be modeled by N electrically identical, parallel units, where N is the total number of the filter pores. One unit consists of a filter pore and its surrounding. The pore is cylindrical (pore length is 13 μm and pore radius is 1 μm), and its symmetry axis is perpendicular to the surface of the filter. The unit itself is assumed to be a cylinder too; its symmetry axis (z axis) coincides with the symmetry axis of the pore, while its cross-sectional area, 254.5 μm^2/unit, is equal to the average filter area per filter pore. The cross section of a unit along the z axis is shown in Figure 2a. The gray area marks the filter pore and the bulk regions on both sides of the filter, while white areas represent the filter around the pore. The double solid line shows the cell membrane. The vertical, z, axis is the symmetry axis of the unit, while the horizontal axis measures the radial distance, r, from the symmetry axis. The unit contains one cell of surface area 137.3 μm^2, which is the average surface

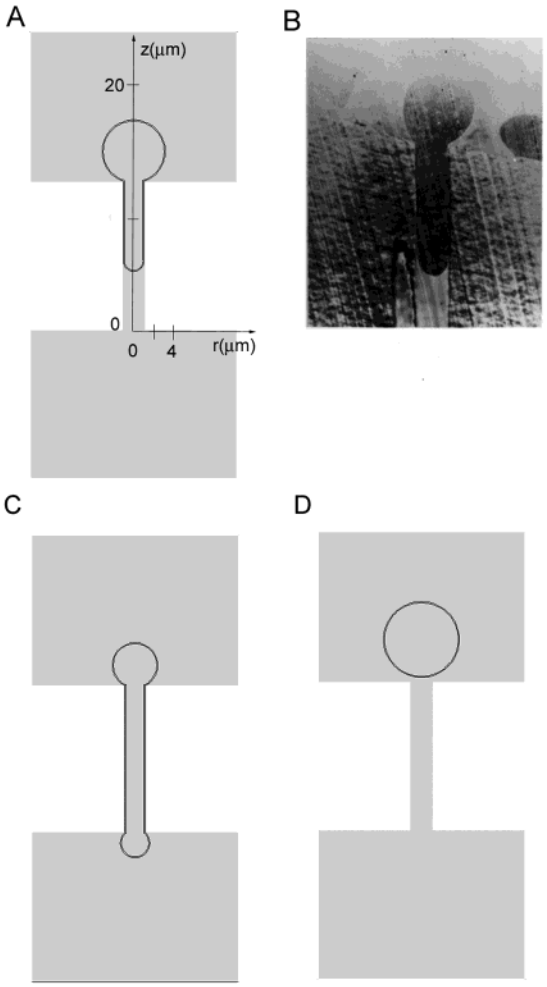

Figure 2. The geometry of a unit of the low-voltage electroporator: (A) schematic of cell partially embedded in the filter pore; (B) transmission electron micrograph of human erythrocyte in the filter pore (the finger length is about 8 μm); (C) schematic of cell fully embedded in the filter pore; (D) schematic of cell out of the filter. White area represents the filter, while gray area marks the bulk solution regions on both sides of the filter and the filter pore. Double solid line shows the cell membrane.

area of an erythrocyte.[23] In Figure 2a,c,d, the cell is partially embedded in the filter pore, fully embedded in the filter pore, and outside the pore, respectively. In each case, the center or symmetry axis of the cell coincides with the z axis of the unit. Outside the filter pore, the cell is assumed to be spherical (Figure 2d). The geometry and location of the cell can be given by its radius ($r_2 = 3.305$ μm) and the coordinate of its center, z_2. When the cell is fully embedded in the filter pore its geometry is assumed to be two truncated spheres connected with a cylindrical tube (Figure 2c). In this case, the geometry and location of the cell can be described by the center and radius of the lower truncated sphere (z_1 and r_1), the outer radius of the tube ($r_t = 0.9$ μm), and the center and radius of the upper truncated sphere (z_2 and r_2). In the case of partially embedded cells, the same parameters define the location and geometry of the cell with the restriction that one of the truncated spheres is a hemisphere (at the tip of the finger) of radius r_t. The part of the cell that is penetrated into the filter pore is called the finger of the cell. The geometry of the cell partially and fully embedded in the filter pore has been confirmed by direct observation.[10,14,17] Figure 2b shows the transmission electron micrograph of a human erythrocyte partially embedded in a filter pore. When physiologic solution is in the extracellular space, the finger length of the embedded erythrocyte cell is about 8 μm (Figure 2b). The flaccidity of the cell and thus the finger length can be modified by changing the salt concentration of the extracellular space.

The geometry of the model system agrees almost completely with the geometry of the LVEP. There are only three aspects in the geometry of the model that differ from the experimental geometry: (1) the membrane thickness of the cell in the model is 0.1 μm, while in reality the thickness of the cell membrane is about 0.01 μm (ref 23); (2) the thickness of the narrow passage between the finger surface and the filter pore wall is 0.1 μm, while in reality it is estimated to be 0.01 μm (see Appendix 1 and ref 17); (3) the thickness of the bulk region on each side of the filter is 13 μm, while in reality it is 1 cm. In the case of this model geometry, we are able to obtain reliable numerical solutions of the partial differential equation of the electric potential. The effect of the deviations 1 and 2 on the transmembrane voltage is negligibly small (see Appendix 2), while deviation 3 can be easily corrected. It was shown by Schmukler[17] that 40% of the applied voltage drops in the filter. Thus in our model calculations, the voltage applied very close to the filter surfaces represents 40% of the voltage applied to the capacitor plates of the LVEP chamber. For example, if 10 V is applied to the LVEP unit, the corresponding voltage applied to the LVEP chamber is 25 V.

2.2. Laplace Equation of the Model of Low-Voltage Electroporator. In this section, the partial differential equation of the electric potential of a unit of the LVEP is described.

2.2.1. Boundary Conditions. In every calculation, the potential applied at $z = 26$ μm, the top of the cylindrical unit, is $u(r,26) = 10$ V, while the applied potential at $z = -13$ μm, the bottom of the cylindrical unit, is $u(r,-13) = 0$ V. A Neumann-type boundary condition was utilized at every other boundary (the wall of the filter pore, the top and bottom surfaces of the filter, the borders to the neighbor units, and the symmetry axis of the unit) because the normal component of the current to each of these boundaries is zero:

$$-\mathbf{n}\cdot(\sigma_f r \nabla u) = \mathbf{n}\cdot\mathbf{j} = 0 \tag{3}$$

where $\mathbf{n}$ is the normal vector to the surface of the boundary, r is the radial distance from the symmetry axis (z-axis), σ_f is the electric conductivity of the extra- and intracellular space, and $\mathbf{j}$ is the current density.

2.2.2. Laplace Equation in Inhomogeneous Medium. The steady-state electric potential in an axially symmetric unit of the LVEP can be determined by solving the following Laplace equation:

$$\frac{\partial}{\partial r}\left(\sigma r \frac{\partial u}{\partial r}\right) + \frac{\partial}{\partial z}\left(\sigma r \frac{\partial u}{\partial z}\right) = 0 \tag{4}$$

2.2.3. The Matching Conditions. The electric conductivity, $\sigma = \sigma(r,z)$, is piecewise continuous and is discontinuous on the outer and inner surfaces of the cell membrane. In our calculations, the same conductivity, σ_f, is taken in the extra- and intracellular regions, while the conductivity of the cell membrane is σ_m. The conductivity ratio of the extra- or intracellular space (0.15 M NaCl) to the human erythrocyte membrane at 25 °C is $\sigma_f/\sigma_m = 2.3 \times 10^4$ (ref 23), while the conductivity of the filter is assumed to be zero. The matching conditions on the membrane surface of normal vector $\mathbf{n}$ are

$$u_f = u_m \tag{5}$$

$$\sigma_f \frac{\partial u_f}{\partial n} = \sigma_m \frac{\partial u_m}{\partial n} \quad (6)$$

2.2.4. Numerical Solution of the Laplace Equation. The numerical solution of the Laplace equation is obtained by using the partial differential equation (PDE) toolbox of the Matlab program (The Math Works, Inc.). This program package is capable of calculating the electric potential, u, at every (r,z) point of our model system, that is, capable of solving a 3D Laplace equation when the system possesses axial symmetry. The program uses the finite element method to solve PDEs. It approximates the two-dimensional, (r,z), computational domain with a union of triangles. The triangles form a mesh. The triangular mesh is automatically generated and can be further refined. Before solving the PDE, to get fine meshes everywhere in the membrane, the program refines the original mesh twice. To solve the Laplace equation, the default parameters of the program are utilized.

3. Results

The electric field in a unit of the LVEP was calculated in the case of different cell positions. The cell position is characterized by z_{min} the z-coordinate of the bottom of the cell. Table 1 lists the geometrical parameters of the cell at each calculated cell position.

In Figures 3−5, the contour plots of the calculated potential, u, are shown at three different cell positions. Because of the LVEP unit's axial symmetry, the calculated potential is symmetric. Thus in Figures 3−5, it is sufficient to show only half of the LVEP unit. In the figures, the consecutive contour lines are 0.5 V apart from each other. To make the contour lines more visible in the membrane and in the narrow passage, the figures are stretched in the direction of the horizontal axis, and thus the shape of the cell is distorted. These plots show that the strongest electric field in the cell membrane is at $r = 0$ and $z = z_{min}$, that is, at the bottom of the cell. Note that there is another local maximum of the density of the contour lines in the membrane at the top of the cell, that is, at $r = 0$ and $z = z_{max}$; however, the respective electric field strength is lower than the field strength at the bottom of the cell membrane.

The transmembrane voltage (the potential at the inner membrane surface minus that at the outer membrane surface) has been calculated along the cell membrane. In Figure 6a−c, the transmembrane voltage, $V(z)$, is plotted against the z coordinate of the membrane segment for cases when the cell is out of the filter and partially and totally embedded in the filter pore, respectively.

4. Discussion

4.1. Transmembrane Voltage. Figure 6a−c shows that, at every considered cell position, the transmembrane potential is maximal at z_{min}, the bottom of the cell. If the cell is fully embedded in the pore, the transmembrane voltage is essentially constant along the cell membrane protruding at the bottom of the filter pore. The transmembrane voltage then linearly decreases along the tubular section of cell. The transmembrane voltage changes sign at the point where the increasing potential along the outer membrane surface becomes equal with the potential inside the cell. The transmembrane voltage stops decreasing and becomes constant along the cell membrane protruding at the top of the filter pore. When the cell is partially embedded in the filter pore, the transmembrane voltage changes similarly along the tubular and protruding section of the cell. The change of the transmembrane voltage along the half-spherical section of the finger is shown in Figure 6d, where the relative transmembrane voltage, $V(\theta)/V(0)$, is plotted against the azimuthal angle, θ (the angle between the z-axis and the vector directed from the center of the hemisphere to the considered membrane segment; $\theta = 0$ at the bottom of the cell). Each curve belongs to a different cell position. When the half-spherical section of the finger protrudes at the bottom of the filter pore ($z_{min} = -0.9\ \mu m$), the relative transmembrane voltage is practically independent of the azimuthal angle (top curve in Figure 6d). However, when the half spherical section is within the filter pore, the relative transmembrane voltage decreases with increasing azimuthal angle, and the decrease becomes steeper with decreasing finger length. It is important to mention, however, that none of the angular dependences are as steep as the $\cos(\theta)$ function (dashed line in Figure 6d), which is the angular dependence of the relative transmembrane voltage of a spherical cell placed in a homogeneous electric field and in an electrically homogeneous medium (see eq 1). The above result suggests that the effective membrane area for electroporation increases with increasing finger length and in the case of long fingers pores can form practically anywhere in the half-spherical section of the finger if V(0) is larger than the critical transmembrane voltage. In the case of 10 V applied to the LVEP unit, that is, $V_{app} = 25$ V applied to the capacitor plates of the LVEP chamber, the transmembrane voltage at the bottom of the finger is larger than the critical voltage at every finger length (see Figure 6b). For comparison, we note that if there is no filter in our electroporator the same applied voltage results in

TABLE 1: Geometrical Parameters of the Cell at Different Cell Positions[a]

z_{min} (μm)	z_1[b] (μm)	r_1[b] (μm)	z_2[c] (μm)	r_2[c] (μm)	cell position
14.822			18.127	3.305	ouside
14.322			17.627	3.305	ouside
13.822			17.127	3.305	ouside
13.322			16.627	3.305	ouside
12.822			16.127	3.305	ouside
11.1	12	0.9	16.03	3.2092	partially embedded
10.1	11	0.9	15.96	3.1382	partially embedded
9.1	10	0.9	15.89	3.0657	partially embedded
8.1	9	0.9	15.81	2.9916	partially embedded
7.1	8	0.9	15.73	2.9153	partially embedded
6.1	7	0.9	15.65	2.8372	partially embedded
5.1	6	0.9	15.57	2.7566	partially embedded
4.1	5	0.9	15.48	2.6738	partially embedded
3.1	4	0.9	15.40	2.5886	partially embedded
2.1	3	0.9	15.29	2.5002	partially embedded
1.1	2	0.9	15.20	2.4085	partially embedded
0.1	1	0.9	15.10	2.3133	partially embedded
−0.9	0	0.9	15.00	2.2141	partially embedded
−1.203 71	−0.26	0.943 71	14.884	2.184 57	fully embedded
−1.517 33	−0.48	1.037 33	14.819	2.133 15	fully embedded
−1.835 13	−0.68	1.155 13	14.763	2.065 23	fully embedded
−2.146 26	−0.86	1.286 26	14.673	1.985 95	fully embedded
−2.465 76	−1.04	1.425 76	14.563	1.886 83	fully embedded
−2.790 84	−1.22	1.570 84	14.417	1.767 84	fully embedded

[a] The surface area of the cell, $S = 137.3\ \mu m^2$, is related to the z_i and r_i parameters as follows:

$$S = \pi(h_1^2 + r_t^2) + 2r_t\pi[(z_2 + r_2 - h_2) - (z_1 - r_1 + h_1)] + \pi(h_2^2 + r_t^2) \quad (8)$$

where the first and third terms are the surface area of the truncated sphere on the bottom and top of the cell, respectively, while the second term is the surface area of the connecting tube of radius r_t. The height of the ith truncated sphere is $h_i = r_i + \sqrt{r_i^2 - r_t^2}$, where $i = 1$ or 2. [b] z_1 and r_1 are the center's z coordinate and the radius of the truncated sphere on the bottom of the cell. [c] z_2 and r_2 are the center's z coordinate and the radius of the truncated sphere on the top of the cell.

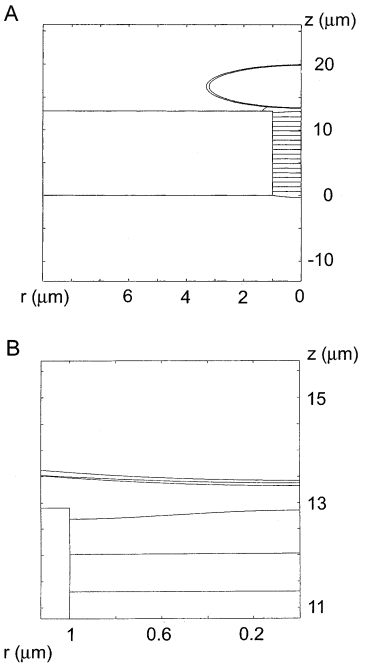

Figure 3. Calculated electric potential when the cell is out of the filter: (A) solution for the entire unit; (B) solution at the bottom of the cell. The contour lines are 0.5 V apart from each other. The cell position is $z_{min} = 13.322$. The voltage applied to the capacitor plates of the LVEP chamber is $V_{app} = 25$ V.

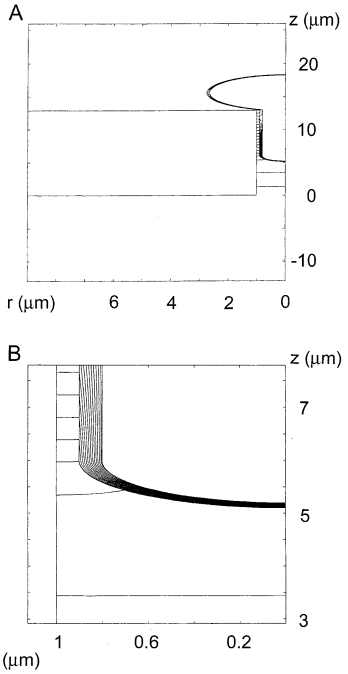

Figure 4. Calculated electric potential when the cell is partially embedded in the filter pore: (A) solution for the entire unit; (B) solution at the bottom of the cell. The contour lines are 0.5 V apart from each other. The cell position is $z_{min} = 5.1$. The voltage applied to the capacitor plates of the LVEP chamber is $V_{app} = 25$ V.

only $V(0) \approx 1.5V_{app}r_2/L = 6.2$ mV (where $r_2 = 3.3$ μm is the radius of the cell and $L = 2$ cm is the spacing between the capacitor plates) transmembrane voltage at the poles of the spherical cell, eq 1. It is the current density amplification (CDA) in the filter pore that produces about a 1000-fold increase of the transmembrane voltage relative to the cell suspension electroporation. CDA estimated by the ratio of the surface area of the filter per pore (254.5 μm^2) and the cross-sectional area

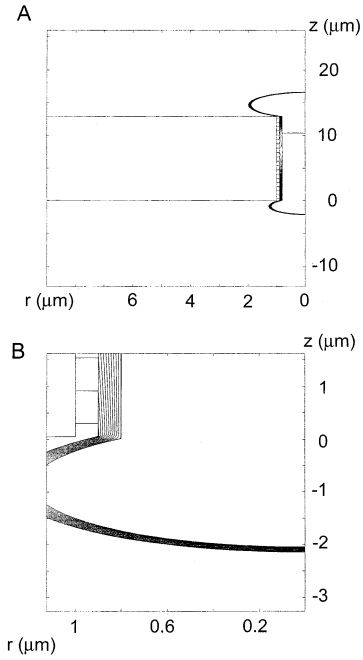

Figure 5. Calculated electric potential when the cell is fully embedded in the filter pore: (A) solution for the entire unit; (B) solution at the bottom of the cell. The contour lines are 0.5 V apart from each other. The cell position is $z_{min} = -2.146\,26$. The voltage applied to the capacitor plates of the LVEP chamber is $V_{app} = 25$ V.

of a narrow passage (0.0753 μm^2, see Appendix 1) is about 3400. Note, that the actual CDA is smaller because part of the electric current flows through the cell membrane (Appendix 2).

The finding that a transmembrane voltage change occurs along the finger of a filter-embedded cell seems somewhat counterintuitive, on the basis of the case of a spherical cell in suspension. The cell membrane of the finger, except for the hemisphere at the end of the finger, is parallel to the direction of the electric field. Our initial assessment, based on angular dependence of the transmembrane voltage along the spherical cell, was that the transmembrane voltage change along the finger length should therefore be zero. However, the finding that the transmembrane voltage changes along the finger can be explained by using concepts from spatial amplification.[24] The differences in boundary conditions between a cell embedded in a pore and a cell in suspension explains this finding. Spatial amplification is defined as the amplification of the electric field across the cell membrane for a cell in suspension at low frequencies when the cell membrane becomes nonconductive. Essentially in spatial amplification, the electric field for the conductive path through the cell integrates along the length of the cell parallel to the field direction. The conduction path through the cell differs from the external conduction pathway because of the presence of cell membranes at each end of the cell. Whereas the voltage drop along the cell in the external medium is linear, uniform and very small, the voltage drop through the cell is not uniform. Nearly the entire voltage drop in the conduction pathway through the cell occurs across the cell membranes at the ends of the cell. This is because, in comparison, there is a negligible voltage drop in the intracellular solution of high conductivity or low resistance. The voltage drop in the external medium is very small, so the potential external to the membrane is essentially constant. The electric field strength across the cell membranes at either end of the cell is amplified by $\sim(^1/_2)$(cell length/membrane thickness). Thus, the transmembrane voltage change for a suspended cell is maximal at the two opposite cell ends. In comparison, for a cell embedded

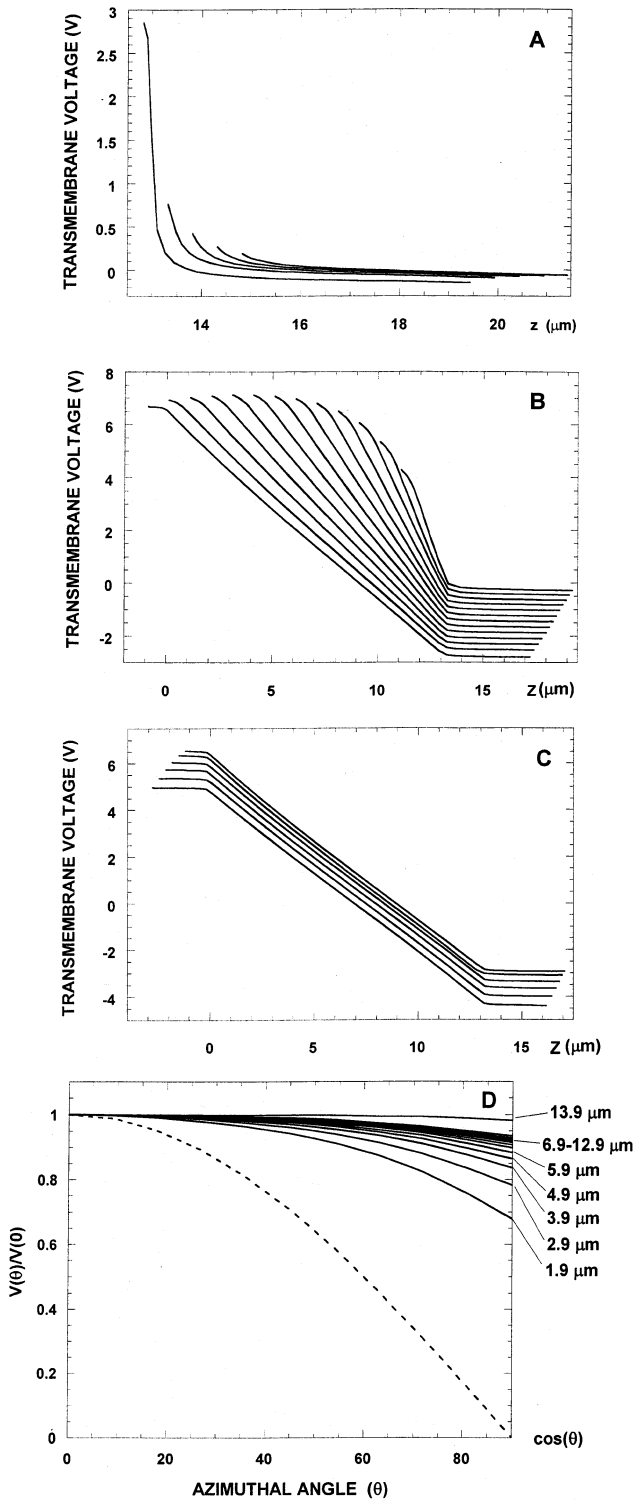

Figure 6. Calculated transmembrane voltage at different cell positions. In Panels A, B, and C, the transmembrane voltage is plotted against the *z* coordinate of the membrane segment. In panel A, the cell is out of the filter. The five different cell positions are listed in Table 1. In panel B, the cell is partially embedded in the filter pore. The 13 different cell positions are listed in Table 1. In panel C, the cell is fully embedded in the filter pore. The six different cell positions are listed in Table 1. Panel D shows the angular dependence of the relative transmembrane voltage, $V(\theta)/V(0)$, in the half-spherical section of the finger of a partially embedded cell. The solid lines from top to bottom belong to cells of decreasing finger length (see labels). The 13 different cell positions are listed in Table 1. The dashed line represents angular dependence of the relative transmembrane voltage in the case of a spherical cell placed into a homogeneous field (see eq 1). The voltage applied to the capacitor plates of the LVEP chamber is $V_{app} = 25$ V.

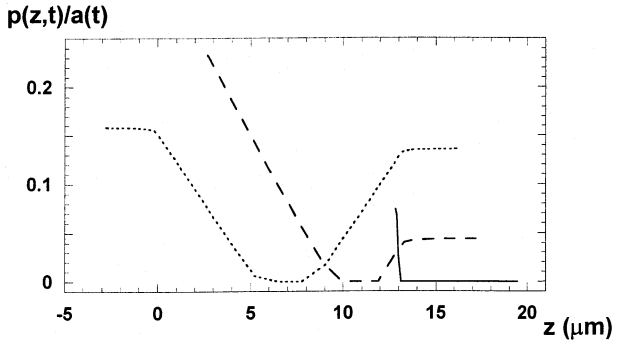

Figure 7. Distribution of electropores along the cell membrane. Spatial distribution of electropores, $p(z,t)/a(t)$, is calculated by eq 7 for three different cell geometries. The solid line represents the cell out of the filter pore, $z_{min} = 12.8$ μm; the dashed line represents the cell partially embedded in the filter pore, $z_{min} = 2.1$ μm; the dotted line represents the cell fully embedded in the filter pore, $z_{min} = -2.79$ μm. The voltage applied to the capacitor plates of the LVEP chamber is $V_{app} = 25$ V. The critical voltage is $V_{cr} = 1$ V.

in a pore, the boundary conditions are reversed with respect to a cell in suspension. In this case, the voltage drop in the extracellular space along the finger in the pore is also linear and uniform, but in contrast to a suspended cell, this voltage drop is significant and not small. The significant external voltage drop results from the high resistance of the narrow passage around the finger in a pore. In this case, at all frequencies, a substantial voltage drop exists in the external conduction pathway. The conduction pathway through the cell is also different compared to the cell suspensions. For an embedded cell, there is a relatively small voltage drop across the membrane of the cell protruding out of the filter pore. This is because the capacitance of the protruding section is about 10 times larger than the capacitance of the hemisphere at the tip of the finger. A very small voltage drop also occurs inside the cell. This means that the situation is different from the situation for a cell suspension in that the voltage drop through the cell before the tip of the finger is small, while the voltage drop in the external pathway is large. This difference produces a significant transmembrane voltage change along the finger that would not occur in cell suspensions. The specialized geometry of a cell embedded in an insulating filter is such that the transmembrane voltage along a cell membrane perpendicular to the filter surface can be nonzero and it can change in response to an applied electric field.

4.2. Distribution of Electropores. Electroporation takes place where the absolute transmembrane voltage of the unporated cell, $|V(z,t)|$, is higher than the critical voltage, V_{cr}. After the charging of the membrane, the temporal and spatial distribution of the electropores in the cell membrane can be given by the following expression:[20−22]

$$p(z,t) = \begin{cases} a(t)\dfrac{|V(z)| - V_{cr}}{V_{appl}} & \text{if } |V(z)| > V_{cr} \\ 0 & \text{otherwise} \end{cases} \qquad (7)$$

where $p(z,t)\,dz$ is the probability of finding a porated region in the membrane segment from z to $z + dz$ and the proportionality factor $a(t)$ gradually increases until the supracritical electric field is on. The spatial distribution of the electropores can be characterized by $p(z,t)/a(t)$. By using the transmembrane voltage curves, $V(z)$, in Figure 6a−c, we have calculated the spatial distribution of the electropores for three different cell geometries (Figure 7). The electropore density is constant along the

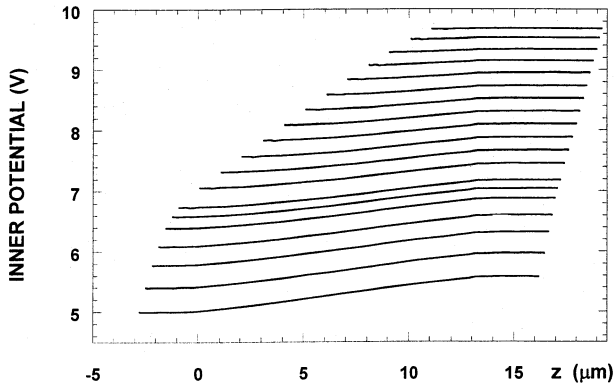

Figure 8. The potential at the inner surface of the membrane plotted against the *z* coordinate of the membrane segment. The curves belong to six fully and 13 partially embedded cell positions listed in Table 1. The *z* coordinate of the leftmost point of each curve is z_{min}, characterizing the cell position. The voltage applied to the capacitor plates of the LVEP chamber is $V_{app} = 25$ V.

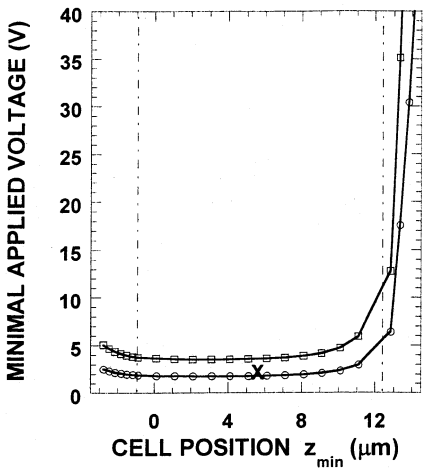

Figure 9. Minimal applied voltage of electroporation. Solid line represents the calculated minimal applied voltage vs cell position. z_{min} values between the vertical dash−dotted lines refer to positions of the cell embedded partially into the filter pore. Open circle and open square marks minimal applied voltage calculated at 0.5 and 1 V critical voltage of electroporation, respectively. The minimal applied voltage observed in LVEP for human erythrocyte is marked by X.

protruding sections of the cell membrane and linearly decreases toward the inside of the filter pore (see dashed and dotted lines in Figure 7). The bottom of the nonembedded cell is electroporated, but then the electropore density sharply drops to zero (solid line in Figure 7). By using Figure 6d, one can also calculate the azimuthal dependence of the pore density in the half-spherical section of the cell finger. The pore density is almost constant in the case of long cell fingers, while for shorter cell fingers the electropore density decreases with increasing azimuthal angle, and the decrease becomes steeper with decreasing finger length.

4.3. Electric Field and Potential. The transmembrane voltage and consequently the electric field strength is highest at the bottom of the cell finger. In the case of 25 V applied to the capacitor plates of the chamber, at the bottom of the finger the through-membrane electric field strength changes from 4.5 to 7×10^5 V/cm, while the finger length increases from 2 to 10 μm. The more embedded the cell is into the filter pore, the lower the potential within the cell becomes. The potential is constant within the protruding section(s) of the cell, while it slightly changes within the finger of the cell (Figure 8). Thus the field strength is negligible in the protruding section(s), and it is less than $460\mathbf{e}_z$ V/cm in the finger. Because of the CDA, the strongest current density of the LVEP can be found in the narrow passage of the filter pore, and similarly in the extracellular space, the field strength is strongest in the narrow passage because the current density is directly proportional to the field strength (Ohm's law). The field strength in the narrow passage close to the membrane surface can be estimated by means of the steepest slope of the transmembrane voltage curves in Figure 6b,c (Appendix 2). When the cell is fully embedded in the filter pore, the field strength in the narrow passage at the membrane surface is $7230\mathbf{e}_z$ V/cm. In the case of partially embedded cells, the electric field in the narrow passage at the membrane surface increases with decreasing finger length from $7230\mathbf{e}_z$ to $23100\mathbf{e}_z$ V/cm. When the geometry of the LVEP unit approaches the real geometry of LVEP, that is, the thickness of the membrane and narrow passage are simultaneously decreased, the relative increase of the electric field strength is significant only inside the cell finger (see Appendix 2). The current density is proportional to the field strength (Ohm's law), and the Joule heating is proportional to the square of the current density. Thus, the Joule heating during the pulse is highest at the narrow passage and negligible in the bulk regions. According to the calculations[16] after three pulses each of amplitude 10 V and duration 30 ms, the Joule heat accumulated in the narrow passage dissipates quickly, within 0.3 ms, toward the bulk regions without causing permanent cell damage. Our experimental results show that after applying the above characterized three pulses only about 2% of the cells die. For comparison, we mention that in SEP during electroporation the Joule heating takes place everywhere in the extracellular space and thus the heat dissipation after the pulse is very slow. The heat transfer through the slowly resealing electropores warms the intracellular space causing eventually permanent cell damage. This explains that in LVEP cells survive even 20 kV/cm local electric field strength, while in SEP 3000 V/cm with pulse duration in the millisecond range is the upper limit of cell survival.[7]

4.4. Minimal Applied Voltage. Because the transmembrane voltage is directly proportional to the applied voltage, one can calculate (from the data in Figure 6) the applied voltage needed to get 0.5−1 V transmembrane voltage at the bottom of the cell. This is the minimal applied voltage needed to electroporate the cell at least at the bottom of the cell. Figure 9 shows the minimal voltage applied on the capacitor plates of the LVEP chamber as a function of the cell position, z_{min}. Open circle and open square marks minimal applied voltage calculated at 0.5 and 1 V critical voltage, respectively. The observed minimal applied voltage for human erythrocyte, marked by X in Figure 9, is within the range of the calculated values. In Figure 9, cell positions between the two vertical dash−dotted lines refer to cells partially embedded in the filter pore. The calculated minimal applied voltage increases steeply with increasing cell-to-filter distance. This theoretical result is similar to the experimental data of Yang et al.[9] They reported a procedure for in situ electroporation of cells grown on microporous membranes of polyethylene terephthalate or polyester (but not pushed into the filter pores) and induced electroporation from as low as 70 V applied voltage. It is important to note that if there is no filter in our LVEP the minimal applied voltage is 4030 V!

4.5. Efficiency of Electroporation. Finally, we point out that the efficiency of electroporation is much higher for fully and partially embedded cells than for cells out of the filter. The efficiency of the electroporation can be characterized by the proportion of the surface of the cell membrane where the

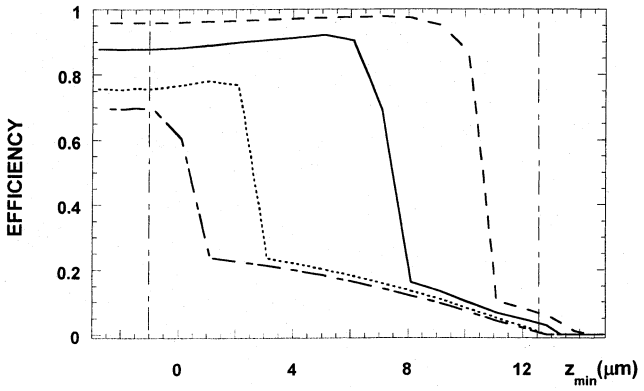

Figure 10. The efficiency of electroporation. The efficiency of the electroporation (i.e., the proportion of the membrane surface area where the critical transmembrane voltage, $V_{cr} = 1$ V, is exceeded) is plotted against z_{min}. The curves belong to the following voltages applied to the capacitor plates of the LVEP chamber: 10 V (dash−dotted line); 12.5 V (dotted line); 25 V (solid line); 75 V (dashed line). z_{min} values between the vertical dash−dotted lines refer to positions of the cell embedded partially into the filter pore. The total surface area of the erythrocyte cell is 137.3 μm^2.

transmembrane voltage exceeds the critical value, V_{cr}. By using Figure 6a−c, one can get the z coordinates of the membrane segments (for a given cell position), where the transmembrane voltage is above the critical voltage. Then one can calculate the surface area of the cell membrane belonging to these z coordinates. The efficiency of the electroporation is this area to the total surface area of the cell. In Figure 10, the calculated efficiency of the electroporation is plotted against the cell position. The curves are calculated at different applied voltages. The efficiency of the electroporation is high, 70−98%, when the transmembrane voltage is above the critical value at both the bottom and the top of the cell. With decreasing finger length (i.e., with increasing z_{min}), the transmembrane voltage decreases at the top of the cell, and when it becomes less than the critical voltage, the efficiency of the electroporation drops considerably. Then the efficiency decreases linearly with decreasing finger length until zero efficiency is attained. At a given cell position, higher applied voltage produces the higher efficiency, and at higher applied voltage, the drop of the efficiency takes place at shorter finger length.

5. Conclusions

In a LVEP, cells are embedded in the pores of a micropore filter. The narrow conductive passages in the filter pores result in a highly inhomogeneous electric field in the electroporator. At as low as 2 V of applied voltage, the field strength becomes 1000−4000 V/cm in each micropore and the transmembrane voltage exceeds the critical voltage of cell electroporation at the tip of the finger, that is, at the bottom of the cell penetrating into the filter pore. The LVEP is ideal for cell transfection with foreign genes. The Joule heat accumulated mainly in the filter pores quickly dissipates toward the bulk solutions of the LVEP chamber before the interior of the embedded cells would warm. Thus the cell survival rate is very high, about 98%. At 25 V applied to the capacitor plates of the LVEP chamber, the transmembrane voltage is higher than the critical value at 87−90% of the cell surface if the cell penetrates further than half length of the filter pore. Because a large percentage of the cell surface can be electroporated, the observed transfection efficiency for the embedded cells is higher than 90%.

Acknowledgment. The authors thank Professor Herman Schwan for his helpful criticism and valuable comments. Dr. Sugár acknowledges Mrs. Gardner's generous support. This work was supported by Pfizer Inc. and by a NIH Grant (Grant 2 R44 HGO1589-02A1).

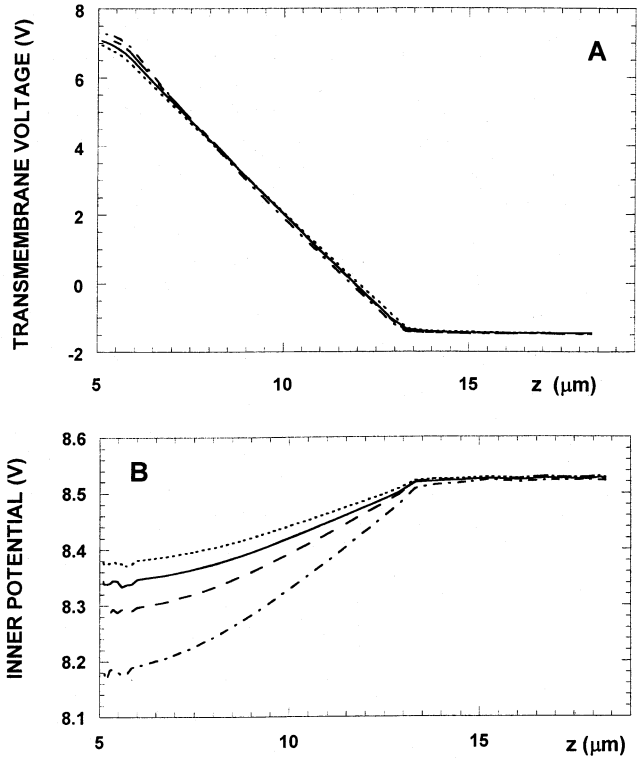

Figure 11. Calculated transmembrane voltage and potential along the membrane at different membrane and narrow passage thicknesses. Narrow passage thicknesses are 0.125 μm (dotted line), 0.1 μm (solid line), 0.075 μm (dashed line), and 0.05 μm (dash−dotted line). At every calculation, the membrane thickness is taken to be equal with the thickness of the narrow passage. $z_{min} = 5.1$ μm. In panel A, the transmembrane voltage is plotted against the z coordinate of the membrane segment. In panel B, the potential at the inner membrane surface is plotted against the z coordinate of the membrane segment. The voltage applied to the capacitor plates of the LVEP chamber is $V_{app} = 25$ V.

Appendix 1

Estimation of the Thickness of the Narrow Passage. The total measured resistance of the electrically parallel narrow passages of the filter pores, that is, the leak resistance, R_L, is 200 Ω and the number of micropores in the filter of radius 0.5 cm is $N_P = 3.3 \times 10^5$.[17] Thus the average resistance of one narrow passage is $R_P = R_L N_P = 6.6 \times 10^7$ Ω. The average cross-sectional area of a narrow passage is $A_P = \rho_f L_P / R_P = 0.0753$ μm^2, where the resistivity of the physiologic solution (0.15 M NaCl) is $\rho_f = 7.1 \times 10^5$ Ω μm and the average length of a narrow passage is $L_P = 7$ μm. The thickness of the narrow passage is expected to be $t_P = r_o - r_i = r_o - \sqrt{r_o^2 - A_P/\pi} = 0.012$ μm, where r_o (1 μm) and r_i are the outer and inner radii of the narrow passage, respectively.

Appendix 2

On the Deviations of the Model's Geometry from the Electroporator's Geometry. In our model, both the membrane and the narrow passage thickness are 10 times larger than the observed values. To investigate the effects of these geometrical parameters on the calculated transmembrane voltages, we simultaneously decreased the thickness of the membrane and the narrow passage first by 25% and then by 50%. The obtained

TABLE 2: Electric Field in the Narrow Passage and in the Cell Finger

membrane thickness (μm)	narrow passage thickness (μm)	E_f (V/cm)	E_p (V/cm)
0.125	0.125	220.4	11 584
0.1	0.1	278.3	11 641
0.075	0.075	361.1	11 725
0.05	0.05	531.9	11 896

transmembrane voltage curves, in Figure 11a, do not show significant deviations from the result obtained in the case of the original model geometry (see solid line in Figure 11a). This is the case because the simultaneous decrease of these two geometrical parameters similarly increases the electric field strength on both sides of the membrane. On one hand, upon narrowing the passage, the current density and the field strength increase in the passage. On the other hand, upon decreasing the membrane thickness, the membrane resistivity decreases and more current flows into the cell finger, that is, the field strength increases in the finger. In Table 2, the calculated field strengths are listed at different thicknesses of the narrow passage and cell membrane. The field strength inside the finger, E_f, is calculated from the steepest slope of the inner potential curve in Figure 11b. The field strength in the narrow passage, E_p, is calculated from the following relationship: $E_p = -dV/dz + E_f$, where dV/dz is the steepest slope of the transmembrane voltage curve in Figure 11a. Note that in the narrow passage the electric field strength increases only by 2% when the thickness of the narrow passage and cell membrane are simultaneously reduced by 50%.

References and Notes

(1) Stämpfli, R. *An. Acad. Bras. Cienc.* **1958**, *30*, 57−63.
(2) Sale, A. J. H.; Hamilton, W. A. *Biochim. Biophys. Acta* **1968**, *163*, 37−43.
(3) Neumann, E.; Rosenheck, K. *J. Membr. Biol.* **1972**, *10*, 279−290.
(4) Zimmermann, U.; Schulz, J.; Pilwat, G. *Biophys. J.* **1973**, *13*, 1005−1013.
(5) Neumann, E.; Schaefer-Ridder, M.; Wang, Y.; Hofschneider, P. H. *EMBO J.* **1982**, *1*, 841−845.
(6) Neumann, E.; Sowers, A. E.; Jordan, C. A. In *Electroporation and Electrofusion in Cell Biology*; Neumann, E., Sowers, A. E., Jordan, C. A., Eds.; Plenum Press: New York and London, 1989.
(7) Friedrich, U.; Stachowicz, N.; Simm, A.; Fuhr, G.; Lucas, K.; Zimmermann, U. *Bioelectrochem. Bioenerg.* **1998**, *47*, 103−111.
(8) Eidsath, A.; Button, D.; Schmukler, R. E. Unpublished work, 1995.
(9) Yang, T. A.; Heiser, W. C.; Sedivy, J. M. *Nucleic Acids Res.* **1995**, *15*, 2803−2810.
(10) Schmukler, R. E. Methods of Electroporation and Electrofusion. U.S. Patent No. 5,173,158, 1992.
(11) Schmukler, R. E. Apparatus for Electroporation and Electrofusion. U.S. Patent No. 5,283,194, 1994.
(12) Schmukler, R. E. *Mater. Res. Soc. Proc.* **1996**, *411*, 45−56.
(13) Huang, Y.; Rubinsky, B. *Biomed. Microdevices* **1999**, *2*, 145−150.
(14) Schmukler, R. E. *Proc. XI Int. Conf. Electr. Bio-Impedance* **2001**, 233−236.
(15) Sugar, I. P.; Schmukler, R. E. *Proc. XI Int. Conf. Electr. Bio-Impedance* **2001**, 149−152.
(16) Schmukler, R. E.; Eidsath, A.; Button, D.; Lindesay, J.; Khizder, K.; Ahmed, A.; Sugar, I. P. Unpublished work, 2003.
(17) Schmukler, R. E. A new technique for measurement of isolated cell impedance. Eng. Sc. D. Thesis, Columbia University, New York, 1981.
(18) Cole, K. S. *Membranes, Ions and Impulses*; University of California Press: Berkeley, CA, 1972.
(19) Schwan, H. P. In *Electroporation and Electrofusion in Cell Biology*; Neumann, E., Sowers, A. E., Jordan, C. A., Eds.; Plenum Press: New York and London, 1989; pp 3−22.
(20) Kinosita, K., Jr.; Ashikawa, I.; Saita, N.; Yoshimura, H.; Itoh, H.; Nagayama, K.; Ikegami, A. *Biophys. J.* **1988**, *53*, 1015−1019.
(21) Hibino, M.; Shigemori, M.; Itoh, H.; Nagayama, K.; Kinosita, K., Jr. *Biophys. J.* **1991**, *59*, 209−220.
(22) Hibino, M.; Itoh, H.; Kinosita, K., Jr. *Biophys. J.* **1993**, *64*, 1789−1800.
(23) Bordi, F.; Cametti, C.; Misasi, R.; De Persio, R. *Eur. Biophys. J.* **1997**, *26*, 215−225.
(24) Takashima, S.; Schwan, H. P. *J. Membr. Biol.* **1974**, *17*, 51−68.